Armenian Journal of Physics, 2010, vol. 3, issue 1, pp. 69–77

ANALYSIS OF TERAHERTZ WAVE PROPAGATION IN GAP PLASMON WAVEGUIDE FORMED BY TWO CYLINDERS

Yu. H. Avetisyan, H. Hakopyan, A. H. Makaryan, and Kh.V.Nerkararyan

Department of Radiophysics, Yerevan State University, Yerevan, 1 Alek Manoogian, Armenia
yuriav@ysu.am

Received February 10, 2010

Abstract - The simple theoretical model is developed to calculate effective index and field distribution of the fundamental TM_0-mode in gap plasmon waveguide formed by two cylindrical surfaces made of gold, doped Si, and polyvinylidene fluoride (PVDF) materials. It is shown that doped Si and PVDF are promising materials for strongly confined THz-wave propagation in gap plasmon waveguide. Though mode confinement in metal waveguide is lower, it is preferable for low-loss undistorted propagation of the broadband THz-pulses.

Key Words: terahertz, plasmon waveguides, THz time-domain spectroscopy

1. Introduction

Recently, plasmon waveguides have attracted much attention due to its potential to guide light in a region beyond the so-called diffraction limit [1-3]. At optical frequencies, many metals support fascinating optical interactions such as surface plasmons polaritons (SPPs) because the dielectric constant of metals in the visible and near-IR regions is predominantly real and negative. It would be greatly advantageous to take concepts of SPP to obtain subwavelength confined guided-wave propagation at terahertz (THz) frequencies. For its unique characters, THz-waves have many applications in scientific research and application fields, such as spectroscopy, free space communication, environmental sensing and medical imaging [4]. During last decade, THz technology has made great progress due to the rapid development of radiation sources [5–7] and detectors [8, 9], while strongly 2-dimentional (D) confined propagation in waveguides is also vitally important to the development of THz technology. Though most studies of SPPs focus on the visible and infrared regions, the SPPs propagation on metal flat surfaces [10, 11] and wires [12, 13] for THz regime is investigated as well.

The main problem of THz-SPPs excitation in metals is large value of plasma frequency, which is defined by $\nu_p^2 = Ne^2/4\pi^2 m_e \varepsilon_0$, where N is the electron density, e electron charge, ε_0 is the vacuum permittivity and m_e electron mass. Since the free electron density in metals is typically of the order of 10^{22} cm^{-3}, the plasma frequency is limited to the visible and ultraviolet regions. At frequencies significantly below the plasma frequency (like the THz range), large negative permittivity strongly prohibits electromagnetic fields from penetration inside a metal, and plasmon excitation on the metal-dielectric interface becomes challenging.

There are different approaches which makes possible to decrease plasma frequency. Recently it was demonstrated that a periodic lattice of thin metallic wires could exhibit a plasma frequency even in microwave [14]. However, many periods of such a structure are required that is a limiting factor to the use of such media in practical applications. Besides, the periodic lattice of thin metallic wires is difficult and expensive to produce. An alternative composite media are structured metal surfaces with periodical groves or holes. This medium is characterized by an effective permittivity that has a plasmon form with a plasma frequency dictated by the geometry of the hole or the groove [15]. However, effective permittivity of the periodical structures is strongly frequency dependent that limit operation bandwidth of plasmonic devices.

In this paper we are focusing on media having plasma frequency well below that of metals, which do not depend on the use of components with dimensions related to the frequency of interest. The doped semiconductors are good alternatives to metals for the excitation of low-frequency plasmons [16]. As the carrier densities in semiconductors are much lower than those in metals, the plasma frequency is much smaller, being typically at mid- or far-infrared frequencies. Therefore, the permittivity of semiconductors at THz is comparable to that of metals at optical frequencies. A decisive advantage of semiconductors is that their carrier density and mobility, and consequently the SPPs, can be easily controlled by thermal or optical excitation of free carriers. However, the doped semiconductors usually have large imaginary part of the complex permittivity that limits SPP propagation length.

It has been known for some time that low-frequency plasmons can be observed in intrinsically conducting polymers [17]. Quite recently porous fiber with ferroelectric polyvinylidene fluoride (PVDF) polymer was proposed as a surface plasmon resonance (SPR) sensor [18]. The PVDF film (usually used in piezoelectric devices) is widely commercially available and it can be easily bonded to different substrates including metals. Moreover, a use of PVDF gives an opportunity to design a fully polymeric THz plasmonic structure, which potentially makes the fabrication process highly suitable for the industrial scale-up.

In this paper we present the characteristics of THz-wave propagation in gap Plasmon Waveguide formed by two Cylindrical Surfaces (PWCS), made of metal, semiconductor, and PVDF (Fig. 1).

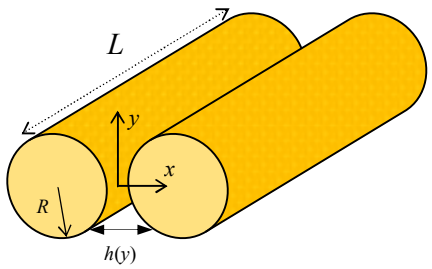

Fig. 1. Schematic view of the waveguide

The analytic description CPP modes in gap PWCS with metal surfaces has been recently obtained in optical regime [19]. Here the simple way to calculate fundamental TM_0 mode sizes and dispersion in THz region is presented. Waveguide is considered as parallel plate waveguide (PPWG) with adiabatically varying distance between plates $h(y)$. It is known [20] that effective refractive index at TM_0 mode in plasmon PPWG is approximately inversely proportional to the distance between plates, $N_{eff} \sim 1/h(y)$. Therefore the model of graded-index dielectric waveguide [21] can be used to calculate THz-wave confinement along the y-axis.

2. Complex permittivity of materials in the THz range

In order to model the gap PWCS, the complex permittivity of cylindrical surfaces (made of metal or doped semiconductors) was assumed to be Drude-like, which corresponds to the approximation of a single energy independent scattering time, τ [22]. This quantity can be related to the dc mobility, μ, by $\mu = e\tau/m^*$. Then the frequency-dependent complex permittivity $\dot{\varepsilon}(\nu) = \varepsilon'(\nu) + i\varepsilon''(\nu)$ takes the form

$$\dot{\varepsilon}(\nu) = \varepsilon_\infty - \frac{\nu_p^2}{\nu(\nu - i\gamma)}, \tag{1}$$

where ν_p is the plasma frequency, γ is the damping rate (inverse scattering time) of the carriers, and ε_∞ is the permittivity at extremely high frequencies that is unity for metals or permittivity of undoped material for semiconductors.

When waveguide's cylinders are made of PVDF, the material dispersion is given by

$$\dot{\varepsilon}(\nu) = \varepsilon_{opt} - \frac{(\varepsilon_{dc} - \varepsilon_{opt})\nu_0^2}{\nu_0^2 - \nu^2 - i\gamma\nu}, \tag{2}$$

where ε_{opt} is the optical dielectric constant, ε_{dc} is the low-frequency (dc) dielectric constant, ν_0 is the frequency of the transverse-optical mode of the material.

Using Eq.(1) with ν_p and γ given in Ref. [23], the complex permittivities of the different high-conductivity metals have been calculated in 0.1–3 THz region. In all cases the negative real part of $\dot{\varepsilon}$ has an order of -10^5. Because THz region is far enough from plasma frequency ν_p the value of ε' is practically independent of frequency. For instance, in gold $-\varepsilon' = 1.14\times10^5$ at 0.1 THz and it is slowly reduced to $-\varepsilon' = 0.94\times10^5$ at 3 THz. Such small dispersion is very attractive for plasmonic waveguides operating in a wide frequency region. The imaginary part of the permittivity in metals (which is related to dissipation) is usually 3–10 times larger than $-\varepsilon'$, whereas in the optical region $-\varepsilon' \gg \varepsilon''$. For gold the ratio $-\varepsilon'/\varepsilon''$ is 0.16 for 1THz, whereas it is $-\varepsilon'/\varepsilon'' = 13$ for 300 THz ($\lambda = 1$ μm).

The doped silicon is chosen to illustrate the behavior of permittivity of the doped semiconductors. The silicon's characteristics in THz range are well established [22] and it is widely available and cheapest semiconductor material. In addition, silicon already used in many studies related to SPP-assisted THz-wave transmission through array of holes [24, 25]. For *n*-doped Si (with $N = 10^{18}$ cm^{-3} and $N = 10^{17}$ cm^{-3}) the dependences of real and imaginary parts of the permittivity on the frequency were calculated with Eq.(1). Because the scattering time of carriers depends on their density, the values of γ have been assumed $\gamma = 1.35$ THz for $N = 10^{17}$ cm^{-3} and $\gamma = 4.1$ THz for $N = 10^{18}$ cm^{-3} in accordance to Baccarani–Ostaja model [26]. The calculated dependencies of $\varepsilon'(\nu)$ and $\varepsilon''(\nu)$ for doped Si with $N = 10^{18}$ cm^{-3} and $N = 10^{17}$ cm^{-3} are presented in Fig.2.

As it is seen in Fig. 2, the lightly doped silicon ($N = 10^{17}$ cm^{-3}) has negative ε' only for $\nu < 0.9$ THz and therefore it cannot support SPP-mode excitation at the interface air–Si for higher frequencies. The doping with free carrier concentration $N = 10^{18}$ cm^{-3} is quite sufficient to have negative real part of $\dot{\varepsilon}$ as far as 3 THz. The last value is close to highest frequency of the common time-domain spectroscopy (TDS) systems.

The calculated dependences of the real and imaginary parts of PVDF permittivity on the frequency are presented in Fig. 3. The following values of $\nu_0 = 0.3$ THz, $\varepsilon_{opt} = 2$, $\varepsilon_{dc} = 50$, and $\gamma = 0.1$ THz have been used in Eq.(2), accordingly to [27].

Fig. 3 shows that plasmon-like SPP excitation may be carried out in the frequency range from 0.4 THz to 1.4 THz. The upper limit is determined by the condition $\varepsilon' < 0$ and lower limit is related to necessity of the relatively small value of ε'', *i.e.* low absorption. Thus the use of PVDF in plasmon THz devices is limited by narrowband applications in the range of approximately 0.4–1.4 THz.

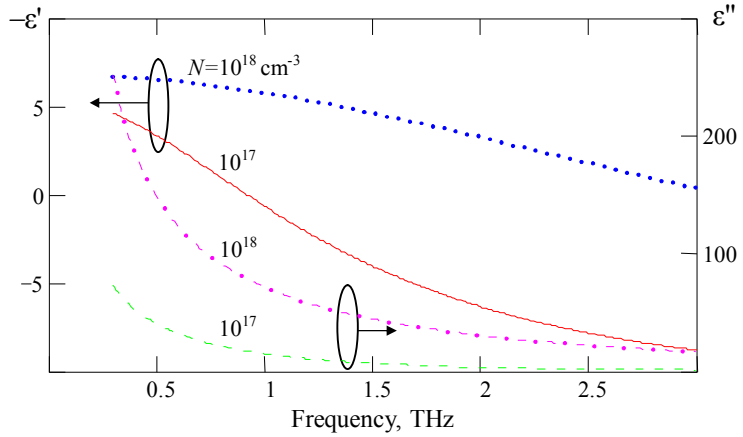

Fig. 2. Dependences of the negative real and imaginary parts of doped Si on the frequency for carrier concentrations N=10^{17}cm^{-3} and N=10^{18}cm^{-3}

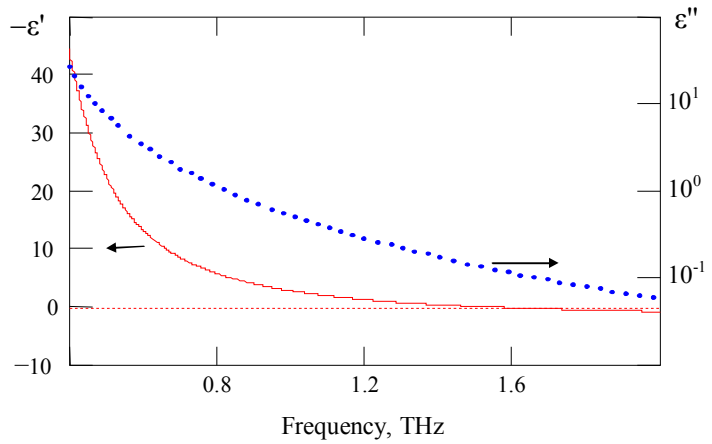

Fig. 3. Dependences of the negative real and imaginary parts of PVDF on the frequency.

3. Effective index of PPWG

In this section, we calculate the effective refractive index $\mathrm{Re}(\dot{n}) = c/\mathrm{v}_{ph}$ (v_{ph} is the phase velocity, c is the velocity of light) of PPWG formed by two infinite parallel plates in the *YZ* plane (see Fig. 1). The plate's separation h_0 is chosen equal to the minimal distance between cylindrical surfaces $h(y=0)$ of the PWCS. Here obtained results will be used in the next section to calculate propagation characteristics of real PWCS.

The dispersion of SPP-mode in PPWG filled with air is given by the expression [2]

$$\tanh\left[\frac{k_0 h_0}{2}\sqrt{\dot{n}^2-1}\right]+\frac{\sqrt{\dot{n}^2-\dot{\varepsilon}^2}}{\dot{\varepsilon}\sqrt{\dot{n}^2-1}}=0, \qquad (3)$$

where $k_0 = 2\pi\nu/c$ is the wavenumber in air, $\dot{\varepsilon}$ is the complex permittivity of the plates material.

Using the calculated (in section 2) complex permittivities $\dot{\varepsilon}$ for doped Si, PVDF, and Au, the numerical solution of (3) is obtained. The dependences of $\Delta = \mathrm{Re}(\dot{n})+1$ and absorption coefficient $\alpha = k_0\,\mathrm{Im}(\dot{n})$ on the frequency for PPWG with $h_0 = 0.1$ mm, and plates made of doped Si ($N = 10^{18}$ cm^{-3}) and gold in the range 0.1–3 THz are presented in Fig. 4. For convenience of the presentation the values corresponding to gold covered PPWG are increased 50 times.

While the absorption coefficient in gold-PPWG is small ($\alpha = 7.6\cdot10^{-3}$ mm^{-1}), the effective refractive index is too close to 1. As we shall be convinced below, the relatively large value of Δ is favorable to have the strong field confinement in lateral direction (along the *y*-axis) of gap PWCS. In PPWG with plates made of doped Si the effective refractive index n more appreciably differs from 1. Though absorption losses are significantly stronger, use of the doped Si can be suitable for chip-scale THz wave guiding.

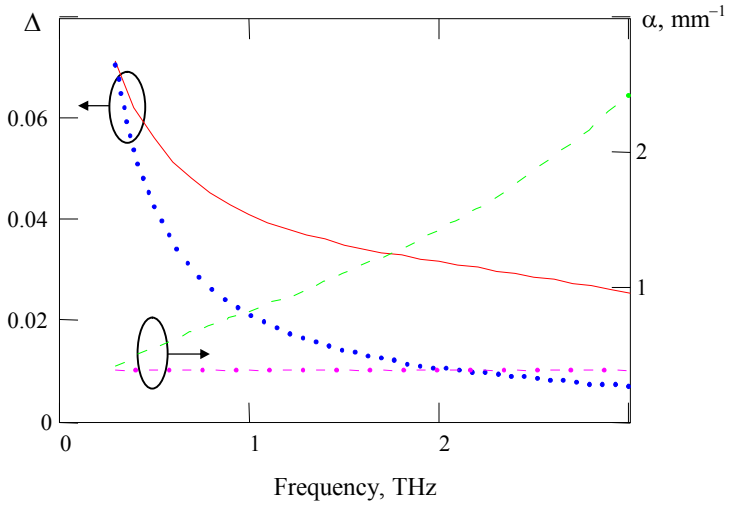

Fig. 4. The dependences of Δ and absorption coefficient α on the frequency for PPWG made of doped Si with $N = 10^{18}$ cm^{-3} (red and green lines) and gold (blue and violet). In the last case calculated values of Δ and α are increased 50 times.

Figure 5 illustrates the dependences of Δ and α on the frequency for PVDF covered PPWG.

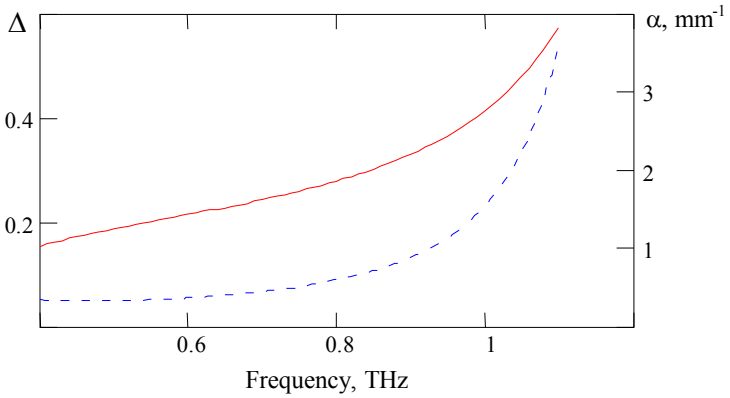

Fig. 5. The dependences of Δ (red line) and absorption coefficient (blue line) on the frequency for PPWG made of PVDF.

It is seen that attenuation of THz-wave is strongly enhanced with growth of the frequency since nearly 1 THz. Hence it is expedient to limit the operation bandwidth of the PVDF-based waveguides by frequencies 0.4–1 THz. The main advantage of PVDF using is relatively large value of Δ that is favorable to obtain small mode size in lateral direction of PWCS.

4. Effective index of PWCS

The effective refractive index $N_{eff} = c/V_{ph}$ (where V_{ph} is the phase velocity in PWCS) of PWCS is calculated by considering it as PPWG with adiabatically varying plate's separation. Using notations shown in Fig. 1, the distance between cylindrical surfaces of PWCS can be written as

$$h(y) = h_0 + \frac{y^2}{R}, \tag{4}$$

where R is the radius of cylinders and condition $|y| << R$ is used.

Based on results of the previous section we can conclude that in all cases $\Delta << 1$. This allows us to simplify Eq. (3) by use the approximate expression $\tanh(x) \approx x$ for sufficiently thin waveguide $h_0 << 1/k_0\Delta^{1/2}$. Then by replacing h_0 with $h(y)$ and using the condition $\dot{\varepsilon} \gg 1$ the following expression for the real part of the refractive index can be obtained:

$$\mathrm{Re}(\dot{n}) = 1 + \frac{1}{k_0 h_0 \sqrt{|\dot{\varepsilon}|}\left(1 + \frac{y^2}{Rh_0}\right)} \sin\frac{\varphi}{2}, \tag{5}$$

where $\varphi = \tan^{-1}(\varepsilon''/|\varepsilon'|)$.

Eq.(5) shows that the refractive index is maximal in the middle of waveguide ($y = 0$) and it is decreased with increase in $|y|$. Therefore the THz beam can be concentrated in the vicinity of the waveguide's middle by similar way that of graded-index dielectric waveguide. The theory of such waveguides is well developed. The analytical expressions for effective refractive index and field distribution were obtained for some profiles of the refractive index, including $n(y) \propto 1/\cosh^2(y)$ [21]. The same profile of the refractive index can be accepted for our case as well. It is follows from Eq.(5) as approximate expression $1 + y^2/Rh_0 \approx \cosh^2\left(y/\sqrt{Rh_0}\right)$ is satisfied if $y^2 << Rh_0$. So using results of Ref. [21], it is easy to obtain that the fundamental TM_0-mode field distribution along the y-axis and effective index N_{eff} of PWCS are given by

$$E_x \propto \cosh^{-s}\left(\frac{y}{Rh_0}\right), \tag{6}$$

$$N_{eff} = \sqrt{1 + \infty\frac{s^2}{Rh_0 k_0^2}}, \tag{7}$$

where

$$s = 0.5\left(\sqrt{1 + \frac{8Rk_0 \sin\frac{\varphi}{2}}{\sqrt{|\dot{\varepsilon}|}}} - 1\right). \tag{8}$$

From Eqs.(6) and (8) follows that small $|\dot{\varepsilon}|$ of the cylinders material is favorable for strongly confined TM_0-mode propagation in waveguide. The TM_0-mode intensity distribution at frequencies $\nu = 0.4$ THz and $\nu = 1$ THz for PWCS (with the radius of cylinders $R = 5$ mm, minimal distance $h_0 = 0.1$ mm) made of doped Si ($N = 10^{18}$ cm^{-3}) and gold are illustrated in Figs. 6a and 6b. The field distribution in PVDF-based waveguide is nearly the same that of PWCS with doped Si and for this

reason it is not shown in Fig. 6a. It is seen that field distributions are frequency dependent as it was generally expected. In case of Si-based PWCS the electrical field is more strongly concentrated in the vicinity of middle of the waveguide (y = 0) than that of Au-based PWCS. It is related to relatively small $|\dot{\varepsilon}|$ for Si material.

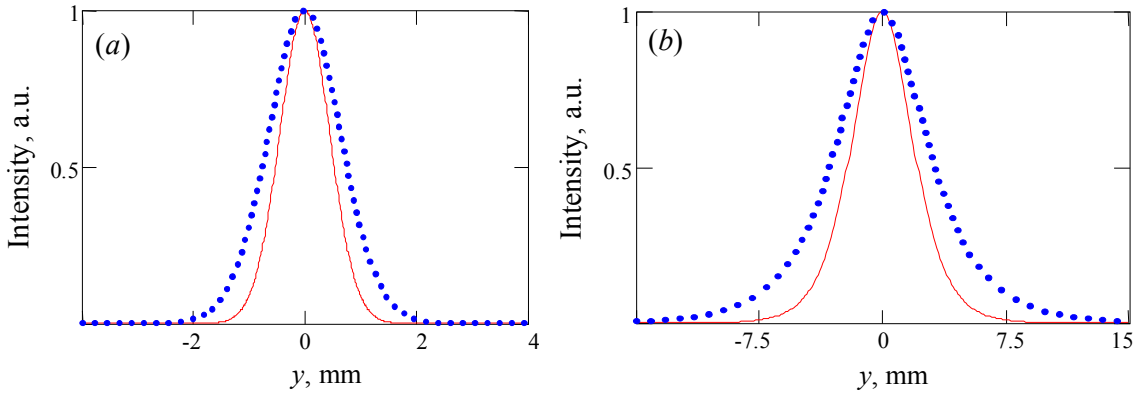

Fig. 6. The fundamental mode intensities distributions in PWCS made of doped Si (*a*) and Au (*b*) at the frequencies 1 THz (red line) and 0.4 THz (blue dotted line).

The dispersion of the effective index of waveguide N_{eff} is very important for applications of PWCS with broadband THz radiation, such as THz-pulse. The calculated dependences $N_{eff} = N_{eff}(\nu)$ are nearly same that of $n = n(\nu)$ for corresponding PPWG (see Fig. 4). For Au-based PWCS the value of N_{eff} is very close to 1 independently of frequency. For Si-based PWCS the value of N_{eff} is 1.076 at 0.1 THz and it is reduced to 1.026 at 3 THz. Even such small dispersion of the waveguide limits its application with broadband THz-pulses. Indeed, after propagating 3 mm distance the delay of spectral components at 0.1 THz and 3 THz is 0.5 ps, which is close to duration of the THz-pulses commonly used in practice.

5. Conclusions

A simple theoretical model is developed to calculate effective index and field distribution of the fundamental TM_0-mode in gap plasmon waveguide formed by two cylindrical surfaces made of gold, doped Si, and polyvinylidene fluoride (PVDF) materials. It is shown that doped Si and PVDF are good candidates for plasmon waveguides supporting strongly confined THz-wave propagation. While mode confinement in metal waveguide is lower, it is preferable for low-loss undistorted propagation of the broadband THz-pulses.

References

1. **K. Tanaka and M. Tanaka,** Appl. Phys. Lett. v. 82, 1158 (2003).
2. *Plasmonic Nanoguides and Circuits*, ed. by **S. Bozhevolnyi**, Pan Stanford, Singapore, 2008.

3. **Y. Matsuzaki, T. Okamoto, M. Haraguchi, M. Fukui, and M. Nakagaki**, Opt. Exp. **16**, 16314 (2008).
4. **M.Tonouchi**, Nat. Photon. **1**, 97 (2007).
5. **T. D. Wang, S. T. Lin, Y. Y. Lin, A. C. Chiang, and Y. C. Huang,** Opt. Express, **16**, 6471 (2008).
6. **K. L. Vodopyanov and Yu. H. Avetisyan**, Opt. Lett. **33**, 2314 (2008).
7. **P. E. Powers, R. A. Alkuwari, J. W. Haus, K. Suizu, and H. Ito,** Opt. Lett. **30**, 640 (2005).
8. **K. Sakai,** Terahertz Optoelectronics, Springer, Berlin, 2005.
9. **A. Leitenstorfer, S. Hunsche, J. Shah, M. C. Nuss, and W. H. Knox,** Appl. Phys. Lett. **74,** 1516 (1999).
10. **T.-I. Jeon and D. Grischkowsky,** Appl. Phys. Lett. **88**, 061113 (2006).
11. **J. F. O'Hara, R. D. Averitt, and A. J. Taylor**, Opt. Express **12**, 6397 (2004).
12. **K. Wang and D. M. Mittleman,** Phys. Rev. Lett. **96**, 157401 (2006).
13. **M. Wächter, M. Nagel, and H. Kurz,** Opt. Express **13**, 10815 (2005).
14. **J. B. Pendry , A. J. Holden, W. J. Stewart, and I. Youngs,** Phys. Rev. Lett., 76, 4773 (1996).
15. **J. B. Pendry, L. M. Moreno, and F. J. Garcia-Vidal,** Science **305**, 847 (2004).
16. **J. G. Rivas, M. Kuttge, H. Kurz, P. H. Bolivar, and J. A. Sánchez-Gil,** Appl. Phys. Lett. **88**, 082106 (2006).
17. **R. Kohlman et al.,** *Handbook of Conducting Polymers*, Ed. Skotheim, Elsenbaumer and Reynolds, Marcel Dekker, New York 1998.
18. **A. Hassani, and M. Skorobogatiy,** in CLEO/QELS-2009 (Optical Society of America, Washington, DC, 2009), CM16.
19. **S. I. Bozhevolnyi and Kh. V. Nerkararyan,** Opt. Express **17**, 10327 (2009).
20. **B. Ghamsari and H. Majedi,** J. Appl. Phys. **104,** 083108 (2008).
21. **H. Kogelnik,** *Guided-Wave Optoelectronics,* 2nd ed. Springer-Verlag, Berlin, 1990.
22. **T.-I. Jeon and D. Grischkowsky,** Phys. Rev. Lett. **78**, 1106 (1997).
23. **M. A. Ordal, R. J. Bell, R. W. Alexander, Jr. L. Long, and M. R. Querry,** Appl. Opt., **24,** 4493 (1985).
24. **J. G. Rivas, C. Schotsch, P. H. Bolivar, and H. Kurz,** Phys. Rev. **B 68**, 201306 (2003).
25. **E. Hendry, F. J. Garcia-Vidal, L. Martin-Moreno, J. G. Rivas, M. Bonn, A. P. Hibbins, and M. J. Lockyear,** Phys. Rev. Lett. **100,** 123901 (2008).
26. **G. Baccarani and P. Ostoja,** Solid-State Electron. **18**, 579 (1975).
27. **T. Furukawa,** Phase Transitions, **18**, 143 (1989).